CHAPTER 8

Dielectric spectroscopy and electro-optical studies of three homologous bent-core mesogens

8.1. Introduction

The dielectric spectroscopy study is based on determining the frequency dependent complex permittivity of a substance and is an essential tool for investigating the dielectric and molecular properties of liquid crystals (LC). It deals with the intermolecular interactions and explores different cooperative relaxation processes at the molecular level [1]. Possible experimental outcomes provide the information about the material properties, molecular dynamics as well as macroscopic phase behavior of the system. The contribution of different relaxation processes to the orientational and distortion polarizations in the complex permittivity can be investigated by monitoring the reorientation of polar and non-polar molecules respectively in response to an oscillating electric field. Different LC phases possess one or more relaxation modes, precisely defines several valuable physical properties of that particular mesophase. Investigation of several relaxation processes by dielectric spectroscopy measurement has been found to be a convenient tool for distinguishing different atypical mesophases such as de Vries [2,3], TGBA [4], several sub-phases of AFLCs [5] etc. and also classifying their molecular structure. Over the past few decades, enormous efforts have been devoted to characterize the relaxation modes in different LC systems comprising of calamitic [6-11], discotic [12], T-shaped [13], chiral [14-16] molecules etc. and also some LC system doped with nanoparticles and porous media [17-20]. Usually, the calamitic nematogens are found to exhibit three dielectric relaxation modes at the high-frequency range [7]. So far from the conventional calamitic compounds, the more exciting behavior is expected to observe in bent-core compounds due to steric hindrance induced by the bent geometry which distorts the symmetry of these molecules. Eventually, in recent years, a number of relaxation modes at the lower frequency region have been discovered in those bent-core systems in comparison to that of calamitic compounds [21,22]. Investigation has also been extended to some binary mixtures consisting of

calamitic and bent-core compounds with different concentrations in order to recognize the possible gradual changes of dielectric parameters from the usual bent-core system to that of the regular calamitic LCs [21,22].

In bent-core compounds, different mesophases exhibit unusual and quite rare characteristics depending on the magnitude and position of bend-angle, the size of the molecules as well as the influence of the terminal chain, linking groups, number of aromatic rings, transverse molecular polarity etc. [23,25]. Although the nematic phase is quite rare in the bent-core compounds, the smectic-like strong short-range local ordering in the nematic phase (namely cybotactic nematic mesophase) has been reported in a number of cases [26-34]. Torgova *et al.* recently synthesized a bent-core molecule based on 1,2,4-oxadiazole as a central unit which exhibits the ferroelectric-like response in the nematic phase due to the existence of smectic-like polar cybotactic clusters [35]. Furthermore, Keith *et al.* have reported a homologous series of the bent-core compounds having a broad range of cybotactic nematic phase along with the higher ordered smectic phases and put forward an idea about the molecular orientations within these phases [36]. More surprisingly, Link *et al.* [37] observed the chirality in layers for the bent-core mesogens due to the combined existence of opposite molecular tilt in adjacent layers and polar vector of the molecules, though they are achiral in nature [38]. Investigation of relaxation modes in such mesophases is an attractive issue because the integrating behavior of the molecules in these phases is much deviating from the usual mesophase behavior. Till now several experimental verifications affirm that the presence of Sm-*C* type polar nano-clusters is responsible for the occurrence of such unusual behavior [39]. Moreover, the macroscopic ferroelectricity has also been observed in these phases [39,40]. Therefore, the presence of these types of unusual mesophases in bent-core compounds is quite encouraging to perform the dielectric spectroscopy study in a broad sense.

In this chapter, the dielectric spectroscopy measurement and the electro-optical investigation has been carried out in detail for three pure achiral bent-core compounds of a homologous series derived from 4-cyanoresorcinol bisbenzoates. The manifestation of the relaxation modes throughout the entire mesomorphic regions has been discussed in light of the molecular associative behavior both in planar and homeotropic alignments. Moreover, a relative comparison of the relaxation modes has been conferred for all of the homologs in accordance with the variation of temperature and chain length as well as the strength of the dipole moments in respective mesophases. To verify the correlation of polar ordering on the relaxation modes, the response to an externally applied DC bias has been measured in these phases. Additionally, the field reversal switching behavior has also been studied to validate the polar ordering of the molecular dipoles and their associative orientation in adjacent layers of the respective mesophases.

8.2. Materials

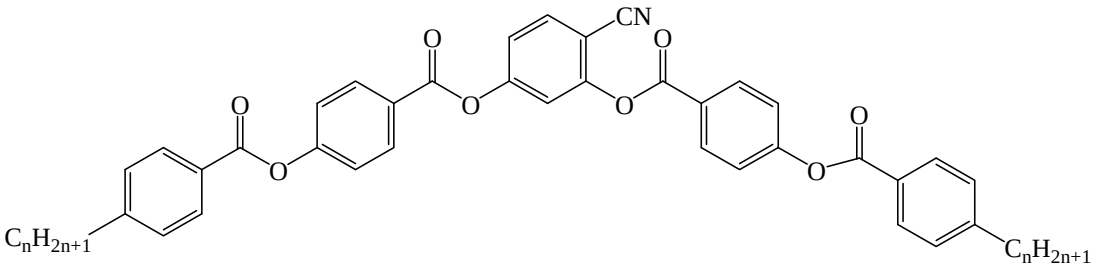

For Compound **1/7**, (n = 7): ***I*** 383 K $\boldsymbol{N_{cybC}}$ 313.3 K **CybC**

For Compound **1/9**, (n = 9)**:** ***I*** 378.6 K $\boldsymbol{N_{cybC}}$ 333.5 K **CybC** 325.4 K **Sm-*C*$_{(I)}$**

For Compound **1/10**, (n = 10)**:** ***I*** 377.6 K $\boldsymbol{N_{cybC}}$ 351.6 K **CybC** 341.6 K **Sm-*C*$_{(I)}$** 330.1 K **Sm-*C*$_{(II)}$**

Investigation on the dielectric spectroscopy has been carried out for three symmetric bent-core compounds of a homologous series of 4-cyanoresorcinol bisbenzoates having terminally substituted alkyl chains

[36,41], synthesized at the Institute of Organic Chemistry, Martine-Luther-University, Halle, Germany. The structural formulae and phase transition scheme of these homologs (**1/7**, **1/9** and **1/10**) are shown above. All three compounds exhibit a highly correlated nematic phase (N_{cybC}) over a wide temperature range followed by a phase (CybC) comprising of elongated but not completely fused strings of cybotactic clusters. In addition, the higher homologs (**1/9** and **1/10)** exhibit one or more tilted smectic phases (Sm-$C_{(I)}$, Sm-$C_{(II)}$). The higher homologous compounds **1/9** and **1/10** exhibits a negative value of dielectric anisotropy, while the compound **1/7** reveals an inversion from positive to negative dielectric anisotropy in the N_{cybC} phase [41].

8.3. Dielectric spectroscopy study

Different dielectric parameters have been explored for the investigated compounds by using an impedance analyzer Agilent 4294A, in the frequency range 40 Hz-15 MHz with a maximum AC voltage of 0.5 V (RMS) to avoid nonlinear responses. Samples were filled into ITO coated LC cells of thickness ~9 μm having both the planar (HG) and homeotropic (HT) configuration. During cooling from the isotropic phase, the real (ε') and the imaginary (ε'') parts of complex dielectric permittivity have been measured in each temperature throughout the entire mesomorphic range at an interval of 1 K, using the well-known procedures as discussed in chapter 2 [42,43]. Obtained dielectric spectrums (ε' and ε'') were fitted with the Havriliak-Negami (H-N) fitting functions [44-47] given below:

$$\varepsilon' = \varepsilon_\infty + \sum_{k=1}^{N} \frac{\delta\varepsilon_k[1 + (2\pi f\tau_k)^{\alpha_k}\cos(\alpha_k\pi/2)]}{[1 + (2\pi f\tau_k)^{2\alpha_k} + 2(2\pi f\tau_k)^{\alpha_k}\cos(\alpha_k\pi/2)]} \tag{8.1}$$

$$\varepsilon'' = \frac{\sigma_0}{(2\pi f)^S} + \sum_{k=1}^{N} \frac{\delta\varepsilon_k[1 + (2\pi f\tau_k)^{\alpha_k}\sin(\alpha_k\pi/2)]}{[1 + (2\pi f\tau_k)^{2\alpha_k} + 2(2\pi f\tau_k)^{\alpha_k}\cos(\alpha_k\pi/2)]} \tag{8.2}$$

where $\delta\varepsilon_k$ is the dielectric strength, ε_∞ is the high-frequency limit of the permittivity, τ_k (= $1/2\pi f_k$) is the relaxation time, f is the corresponding

relaxation frequency, α_k and β_k are shape parameters describing the symmetric and non-symmetric broadness of the dielectric dispersion curve respectively, ranging between 0 and 1, and k is the number of relaxation processes. However, σ_0 is related to the DC conductivity, and S is a fitting parameter responsible for the slope of the conductivity.

The frequency-dependent real (ε') and imaginary (ε'') parts of the complex permittivity for the compound **1/7 (**at a particular temperature 348 K) have been displayed in Fig. 8.1(a) and Fig. 8.1(b) for the planar (HG) and homeotropic (HT) alignments respectively. Corresponding temperature dependence of the relaxation frequency (f_R) for different relaxation processes are presented in Fig. 8.2(a,b) for both cell configurations, while the obtained dielectric strengths ($\delta\varepsilon$) are shown in Fig. 8.2(c,d).

The dielectric spectra in Fig. 8.1(a) for HG cell configuration clearly indicates two relaxation peaks, one is marked as P_1, appeared in a few kHz ranges and a high-frequency peak marked as P_{ITO} which is independent of temperature and arises due to the influence of ITO resistance in series with the cell capacitance. Conversely, in the case of HT cell, corresponding relaxation modes are depicted in Fig. 8.1(b), representing a high-frequency peak H_{ITO} along with two temperature-dependent peaks (H_1, H_2) appeared at the lower frequency side of the H_{ITO}. Noticeably, the P_1 mode in HG cell has a smaller value of dielectric strength ($\delta\varepsilon$) throughout the whole cybotactic nematic (N_{CybC}) phase. On the other hand, the H_1 mode in HT cell has appeared at a lower frequency range with a smaller value of dielectric strength which is weakly sensitive to the externally applied bias field. Thus, the reason behind the appearance of P_1 and H_1 modes may be regarded as the rotation of the molecules around their long and short axes respectively [48]. Hence, in case of transverse component (HG cell), the effect of the molecular rotation around the long axis leads to a high-frequency relaxation peak, while in longitudinal

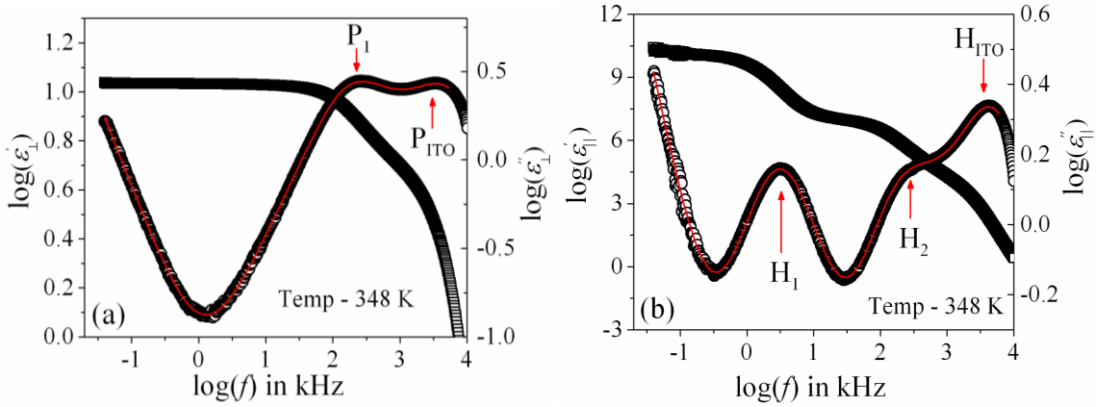

Figure 8.1. Frequency dependence of the real (ε') and imaginary (ε'') parts of the permittivity for compound **1/7** in (a) HG or planar and (b) HT or homeotropic cell configurations. Red solid lines represent the fitting curve to data points with Eq. (8.2).

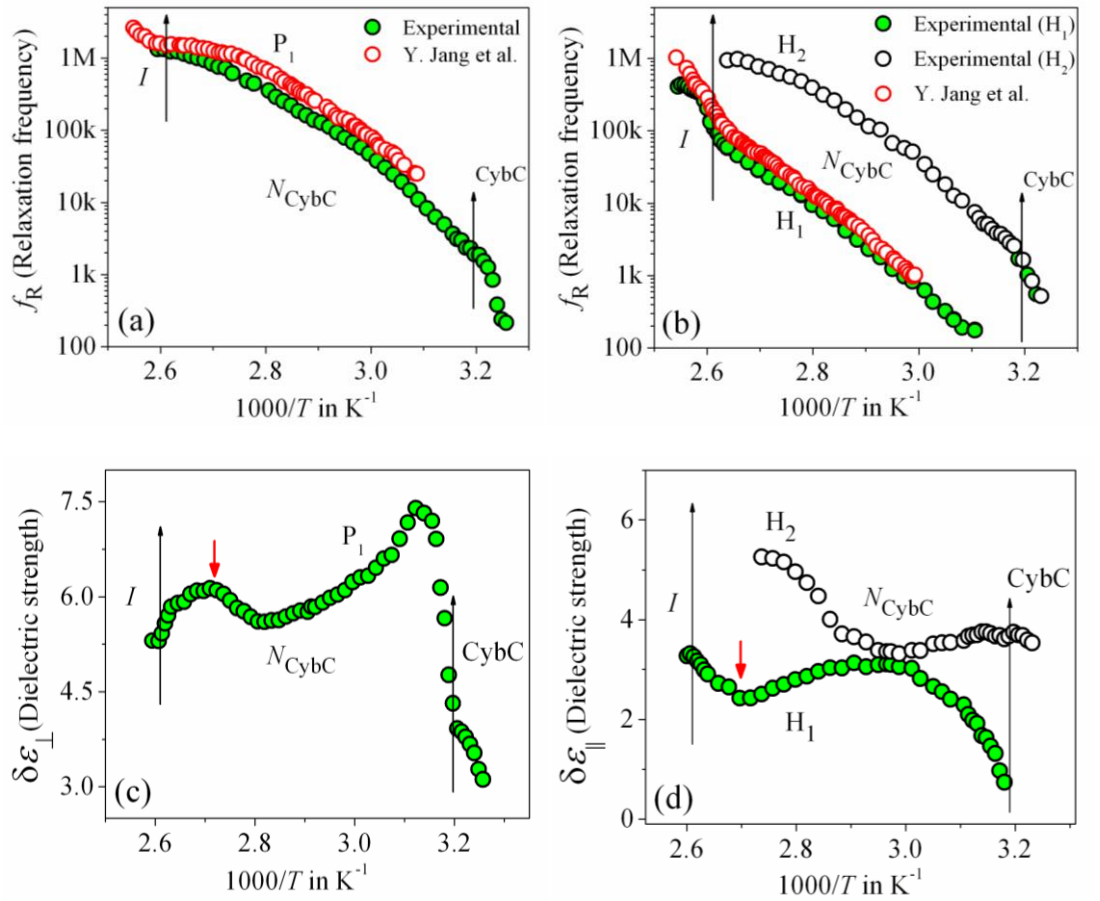

Figure 8.2. Temperature dependence of relaxation frequency (f_R) and dielectric strength ($\delta\varepsilon$) for compound **1/7** in (a,c) planar and (b,d) homeotropic cells respectively. Vertical arrows define corresponding phase transition temperatures.

component (HT cell) the same about short axis leads to a low-frequency relaxation peak. Similar observation has been reported by Jang *et al.* [48] in planar and homeotropic orientations. The extracted experimental values for the relaxation frequency (f_R) in the present system agrees quite well with others in both the cell alignments as represented in Fig. 8.2(a,b). However, in addition to H_1 relaxation mode in HT cell, the present system offers a second mode (H_2) at higher frequency region. By lowering the temperature, the value of relaxation frequency (f_R) for this mode progressively decreases towards the lower frequency region throughout the N_{CybC} phase. However, the value of f_R is found to be nearly equal to that of the P_1 mode in the planar configuration and also reveals a weak dependence upon the applied biasing field. Hence, it can be assumed that due to the superposition of different independent rotation of polar molecules around their long axis or around the principle director implements this relaxation mode. Earlier investigations of Tadapatri *et al.* for a similar type of molecule with alkoxy terminal chain, also support the present outcomes [49,50]. This type of high-frequency relaxation mode in longitudinal component appears in GHz range for usual calamitics but downshift of this mode in the bent-core compound may be assigned due to molecular size and very high viscosity of the sample. Moreover, a quite analogous identification of three relaxation peaks (H_1, H_2 in HT cell, and P_1 in HG cell) has also been observed in some bent-core nematic as well as in mixtures with calamitics [51-53]. Furthermore, in the present investigation, the dielectric strength ($\delta\varepsilon$) for the P_1 and H_1 modes has found to demonstrate an anomalous behavior at a region below ~15 K from the isotropic–nematic (I–N_{CybC}) phase transition as shown in Fig. 8.2(c,d). The value of $\delta\varepsilon$ is found to initially increase in HG cell while it reduces in HT cell followed by the I–N_{CybC} phase transition. Surprisingly, near the temperature 365 K (marked with red arrow) both of the data for $\delta\varepsilon$ has been observed to reveal a kink and follow the opposite pattern thereafter. The previous investigation of this compound also unveils an

inversion in positive to negative dielectric anisotropy at ~18 K below the *I*–N_{CybC} phase transition temperature [41]. Due to the presence of Sm-*C* type polar nano-clusters in the nematic phase and the mutual alignment of these clusters leads to such a behavior. However, it has been reported that this inversion of dielectric anisotropy is also dependent on frequency and the nature of corresponding crossover frequency is highly non-Arrhenius type at lower temperature [48,54]. Recently, Jang *et al.* explained that inversion by assuming the value of anisotropic Kirkwood correlation factors ($g_{\parallel}$ and $g_{\perp}$) not equal to 1, rather $g_{\parallel}$ decreases and $g_{\perp}$ increases than unity, *i.e.*, $g_{\parallel} < 1$ and $g_{\perp} > 1$ [54].

The frequency-dependent imaginary (ε'') part of the complex permittivity for the second homologous compound **1/9** is shown in Fig. 8.3(a,b) for both the HG and HT cell alignments respectively. Corresponding temperature-dependent relaxation frequencies (f_R) and the dielectric strengths ($\delta\varepsilon$) are plotted in Fig. 8.4(a,b) and Fig. 8.4(c,d) respectively, as a function of 1000/T.

In this case, the frequency dependent imaginary component of permittivity (ε'') for HG cell is characterized by a single relaxation peak (P_1). On the other hand in HT cell, the dielectric modes are portrayed by two relaxation peaks- H_1 and H_2. The H_1 mode appears at a frequency about 100 kHz and found to decrease throughout in N_{CybC} phase by lowering the temperature. However, the other mode (H_2) arises near the N_{CybC}–CybC phase transition but at relatively high-frequency region than H_1 mode. On a close look to the temperature variation of relaxation frequency for P_1 mode, it reveals an almost same variation as observed in the planar-aligned compound **1/7**. Moreover, it has been found that the dielectric strength ($\delta\varepsilon$) of this peak is strongly dependent on temperature, *i.e.*, it gradually increases its magnitude in the nematic phase with decreasing the temperature. Further lowering the temperature, the value of $\delta\varepsilon$ decreases sharply in the Sm-$C_{(I)}$ phase via the

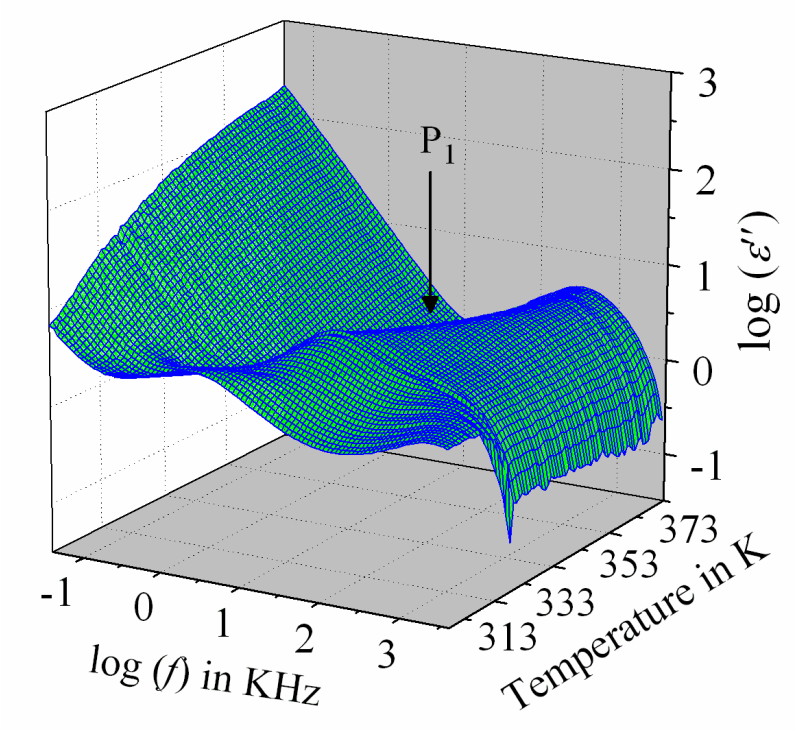

(a)

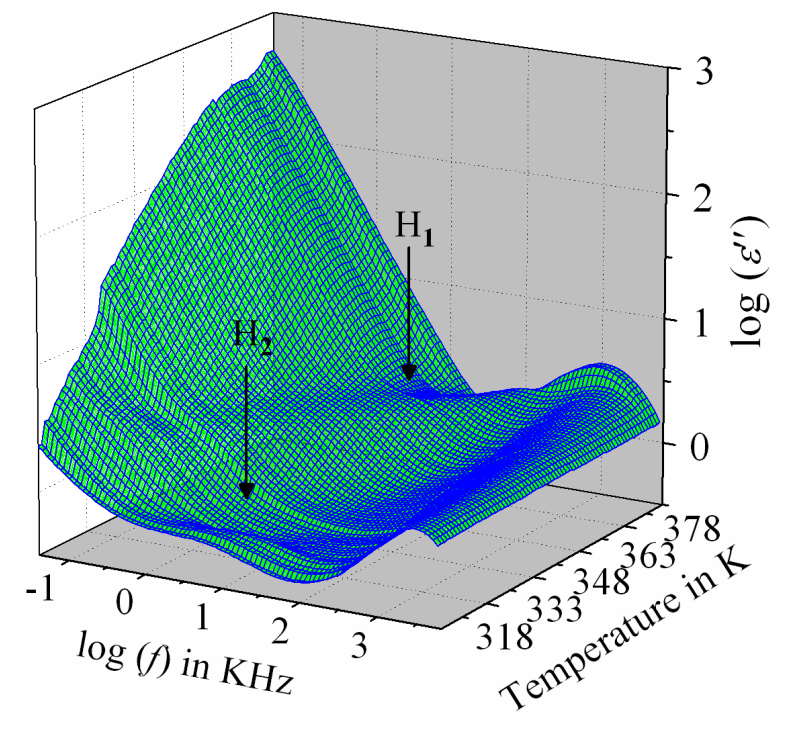

(b)

Figure 8.3. Frequency dependence of the imaginary (ε'') parts of the permittivity for compound **1/9** in (a) HG or planar and (b) HT or homeotropic cell configurations.

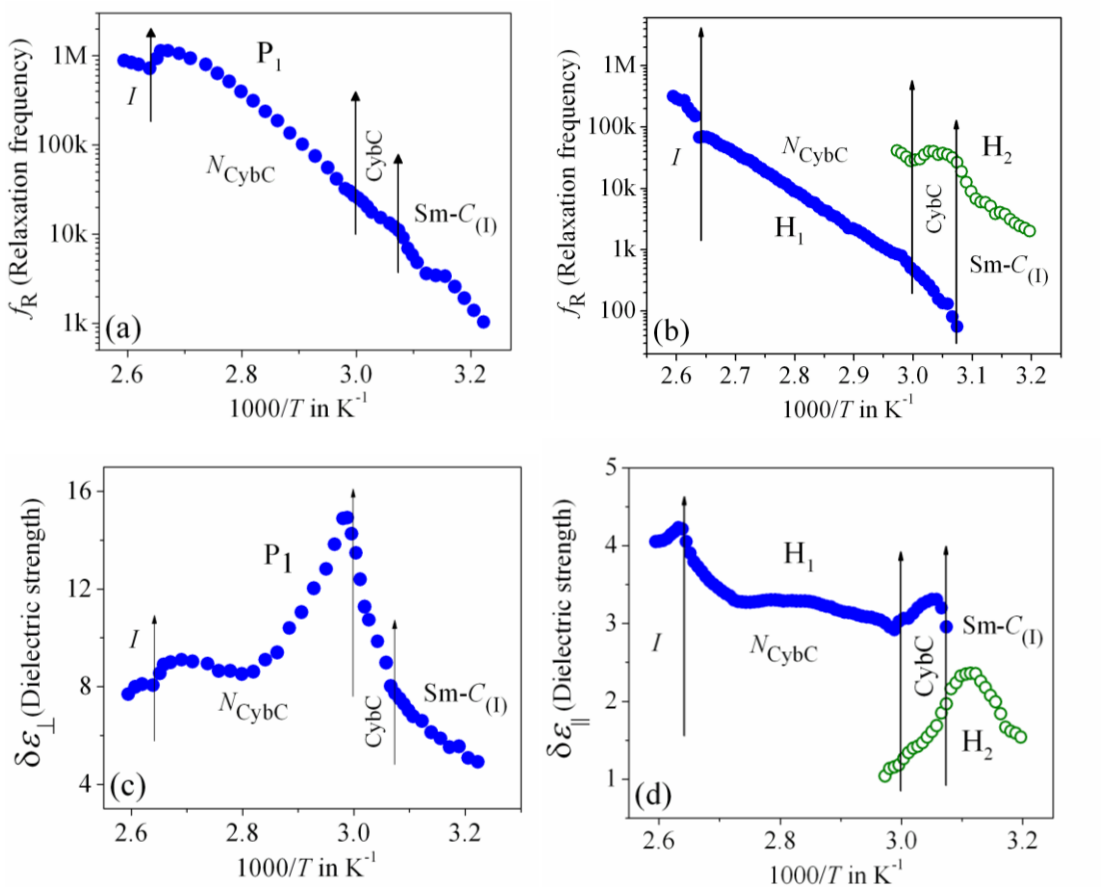

Figure 8.4. Temperature dependence of relaxation frequency (f_R) and dielectric strength ($\delta\varepsilon$) for compound **1/9** in (a,c) planar and (b,d) homeotropic cells respectively. Vertical arrows define the corresponding phase transition temperatures.

CybC phase. A similar type of observation for the dielectric strength has been reported by Eremin *et al.* at the transition to a para-electric to anti-ferroelectric Sm-*C* phase transition for a bent-core compound [55]. In the N_{CybC} phase there exist a number of small-sized cybotactic clusters with Sm-*C* type layer structure which correspond to a strong short-range correlation among the molecules and the cluster size is being elongated by lowering the temperature [36]. Thus, the appearance of this mode can be assigned due to rotation of molecules within the clusters around the long axis of the director in the nematic phase. However, it can be considered that the anti-parallel correlation of the molecular dipoles along the long axis essentially affecting this mode in Sm-$C_{(I)}$ phase. The CybC phase is a phase comprising elongated but not completely

fused strings of cybotactic clusters, the anti-parallel dipolar alignments are observed to be initiated from the N_{CybC}–CybC phase transition. Although, the compound **1/9** posses a larger molecular size and dimension of the cluster in comparison to that of the compound **1/7**, the temperature-dependent variation of the cluster size as well as the molecular tilt plays a significant role in the entire N_{CybC} mesophase. The tilt angles of these molecules enhance from 15^o in N_{CybC} phase to 32^o in a perfectly aligned Sm-$C_{(I)}$ phase through the CybC phase in which molecular tilt angle is 28^o [36]. Therefore, it can be assumed that in the N_{CybC} phase the assembly of molecular dipole moments associated with Sm-*C* type polar clusters forms a ferroelectric type of alignment in neighboring layers and thereby increases the strength of the relaxation modes by decreasing the temperature followed by the elongation of the cluster size. Consequently, the value of $\delta\varepsilon$ enhances gradually in the N_{CybC} phase. Further lowering the temperature, the clusters are fused into elongated ribbon-like aggregates in the CybC phase and orient the dipole moments in such a way that an anti-ferroelectric type of ordering of the dipoles develops in adjacent layers. The strong dipole-dipole interaction favors to align the molecular dipole moments in adjacent layers with an anti-parallel ordering. This anti-ferroelectric type of orientation has been observed to continue throughout the Sm-$C_{(I)}$ phase which causes an effective decrease in $\delta\varepsilon$ value in the CybC and Sm-$C_{(I)}$ phases. Almost identical type of behavior has been observed by Guo *et al.* for a bent-core compound at the transition from Sm-AP_R phase to anti-ferroelectric Sm-AP_A phase [56]. Again, this mode is sensitive to the external bias field. From the Fig. 8.5(a) it is clearly evident that the strength of the mode P_1 is further increases by increasing the bias field without any change of f_R. This indicates that this mode (P_1) develops due to the molecular rotation about the long axis and additionally influenced by the local anti-ferroelectric ordering of the molecular dipoles in adjacent layers. A complete realization of this issue has been drawn from the field-induced polarization technique as described later. Further increasing the field strength, the trivial appearance of an additional

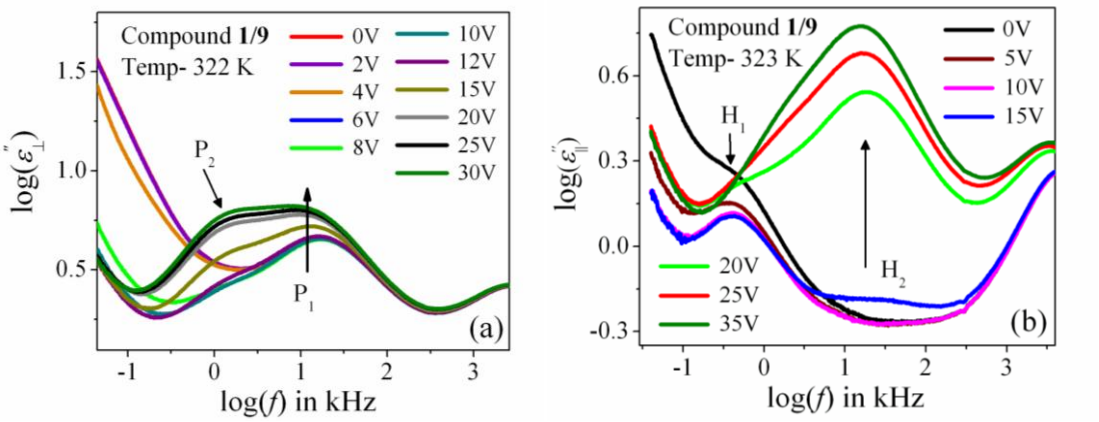

Figure 8.5. The variation of frequency-dependent imaginary (ε'') part of permittivity with the bias voltage for compound **1/9** in (a) planar and (b) the homeotropic alignment cells.

peak (P_2) has been observed in the Sm-$C_{(I)}$ phase at a lower frequency side. This suggests that there also exist an additional rotational motion of the molecules around the short axis or bow axis, as well as it has an effect of local polar ordering that has been apparently recognized after the application of external voltage. Nevertheless, in case of HT cell, both H_1 and H_2 peaks have a relatively smaller dielectric strength than P_1 mode and having a weak temperature dependency. However, a noticeable change in $\delta\varepsilon$ has been found in the CybC and Sm-$C_{(I)}$ phases. The relaxation frequency for H_1 mode is quite similar to that of the compound **1/7** in N_{CybC} phase. Therefore, this mode is also assigned to the molecular relaxation, appearing due to the end-over-end rotation of molecules around their short axis or bow axis. An identical observation has been reported in a bent-core compound having similar molecular core structure but with alkoxy terminal chain [50]. Moreover, the signature of the mode H_2 has found from the CybC mesophase relatively at higher frequency region than H_1 and it extends to the entire Sm-$C_{(I)}$ phase. Interestingly, the strength of this mode is highly sensitive to the external bias field, *i.e.*, the value of $\delta\varepsilon$ increases with increasing the bias voltage, while it is very small in absence of the field as observed from Fig. 8.5(b). Hence, this mode can be attributed to a collective mode of relaxation in which anti-

ferroelectric domains of polar molecules in Sm-$C_{(I)}$ phase transforms to ferroelectric domains by inducing external DC field, thereby effectively increases the strength. It has been observed from Fig. 8.5 that the electric field response of relaxation modes is too much strong in HT cell than that of the HG cell. It demonstrates that the contribution of effective molecular dipole moments in HT cell is greater compare to HG cell subsequent to the application of bias voltage. Hence, due to the anti-parallel alignment of the molecular dipoles, the effective dielectric strength initially shows much smaller value in absence of the field. On increasing the external field, the dipolar groups tend to reorient progressively parallel to the field direction, while the long molecular axes remain randomly distributed around the field direction. This results an enhancement of the dielectric strength along the field direction with increasing the field strength. However, in case of HG cell, the component of the dipole moment parallel to the field direction is too weak compared to that in HT cell and therefore, not so sensitive to the external bias field.

The frequency-dependent imaginary (ε'') part of the dielectric permittivity for the higher homologue **1/10** at different temperature is shown in Fig. 8.6(a,b) for both the HG and HT cells respectively. Corresponding temperature-dependent relaxation frequencies (f_R) and the dielectric strengths ($\delta\varepsilon$) are plotted in Fig. 8.7(a,b) and Fig. 8.7(c,d) respectively, as a function of 1000/T.

In planar configuration, a high-frequency peak (P_1) appeared in a frequency range identical to the lower homologous compounds, with a relatively large value of $\delta\varepsilon$. During cooling from the isotropic phase, the value of $\delta\varepsilon$ gradually increases in N_{CybC} phase and found to decrease in the CybC and Sm-$C_{(I)}$ phases. This observation is quite similar to the compound **1/9** in HG cell. Moreover, in the Sm-$C_{(I)}$ phase, an additional relaxation mode (P_2) with a very close value of f_R has been observed. By applying an external bias field,

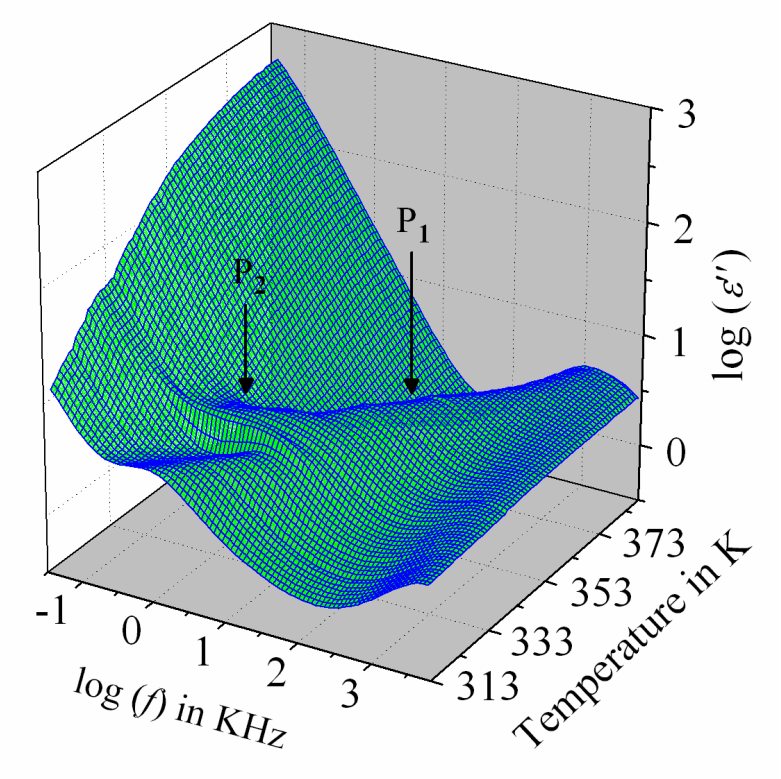

(a)

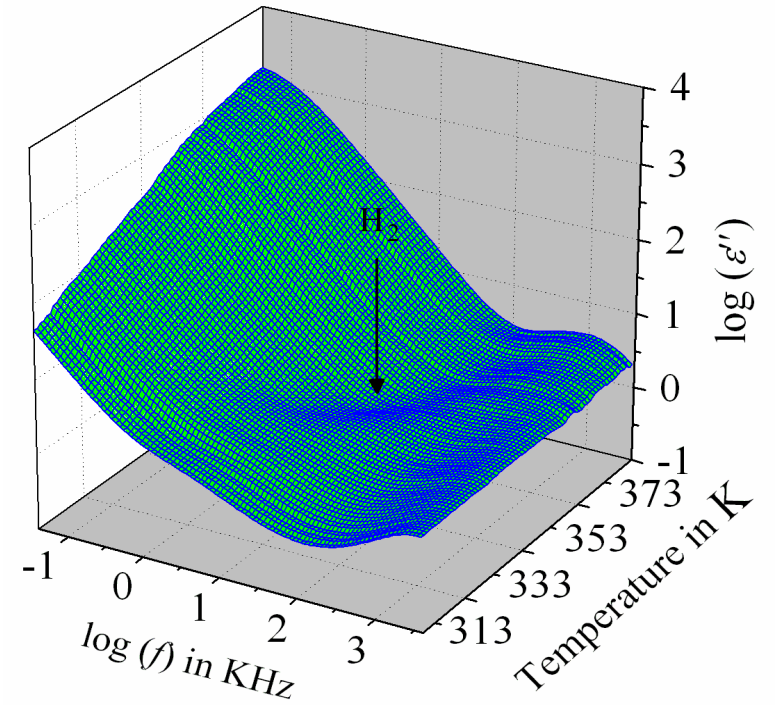

(b)

Figure 8.6. Frequency dependence of the imaginary (ε'') parts of the complex permittivity for compound **1/10** in (a) HG or planar and (b) HT or homeotropic configuration cells.

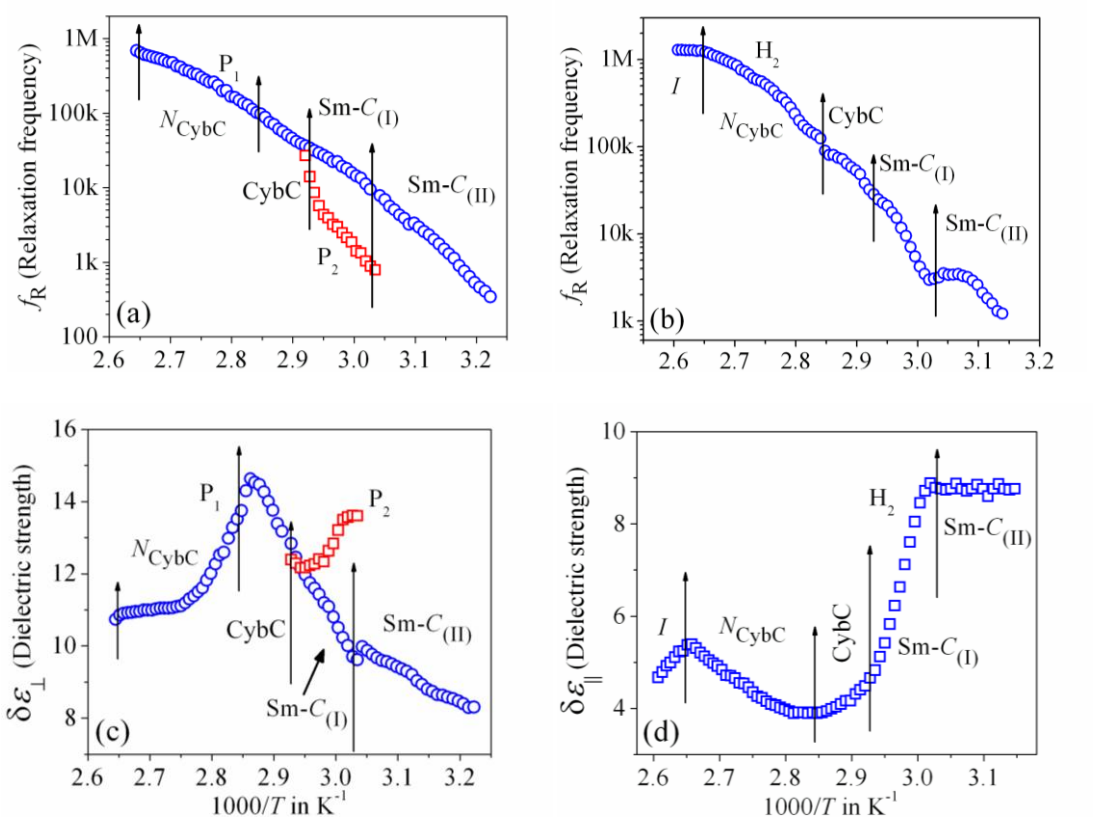

Figure 8.7. Temperature dependence of relaxation frequency (f_R) and dielectric strength ($\delta\varepsilon$) for the compound **1/10** in (a,c) planar and (b,d) homeotropic cells respectively. Vertical arrows define the corresponding phase transition temperatures.

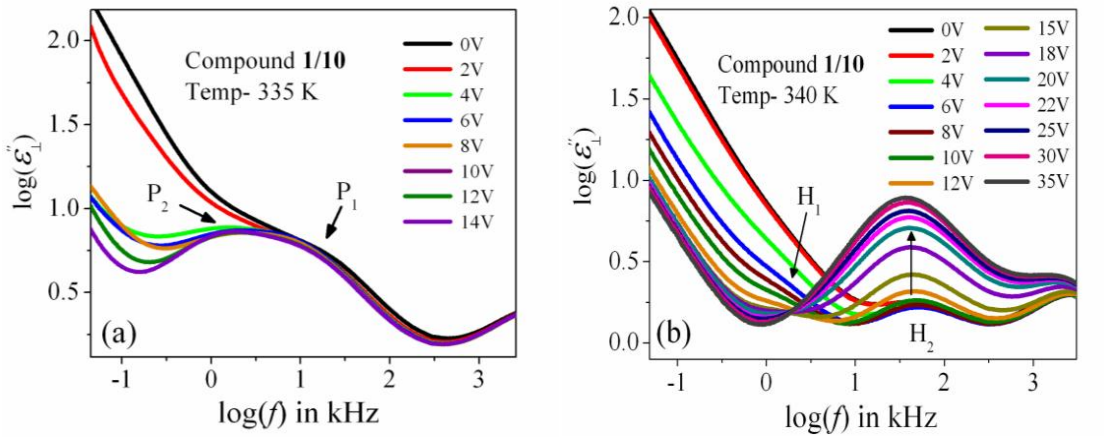

Figure 8.8. The variation of frequency-dependent imaginary (ε'') part of the complex permittivity with the bias voltage for compound **1/10** in (a) planar and (b) the homeotropic alignment cells.

these two modes can be resolved clearly (See Fig. 8.8(a)). On further cooling, the P_1 mode persists to the lower temperature Sm-$C_{(II)}$ phase. Therefore, similar to the compound **1/9**, the P_1 mode in the compound **1/10** can be ascribed as the molecular mode in the N_{CybC} phase, while in tilted Sm-$C_{(I)}$ phase, the orientation of the molecules in anti-parallel fashion with a greater tilt angle, describing a collective process of relaxation. Conversely, in the homeotropic cell, a single relaxation mode (H_2) has been observed throughout the whole mesomorphic range rather than the two relaxation modes (H_1 and H_2) as observed in lower homologous compounds (**1/7** and **1/9**). However, the strength of this mode is comparatively lower than that of the HG cell. Although, during cooling, the value of the dielectric strength slightly decreases in N_{CybC} phase, it enhances further in the CybC and Sm-$C_{(I)}$ phases. Furthermore, the $\delta\varepsilon$ value remains almost constant at the Sm-$C_{(II)}$ phase, in which the molecules are considered to be organized in a quite close-packed structure. Interestingly, the strength of this mode in the Sm-$C_{(I)}$ phase sharply increases with the applied biasing field as shown in Fig. 8.8(b). Notably, on applying the bias voltage, the first longitudinal mode (H_1) is observed minutely at a lower frequency region than H_2, which has been found to appear predominantly in the lower homologous compounds without any bias voltage. It can be explained that due to the enhancement of the molecular length in compound **1/10**, the terminal chains easily escaped into the surface boundary and produce the aliphatic excrescences around the cluster [36]. Moreover, combination of the steric interaction and dipole-dipole interaction favors to orient the terminal chains parallel to the layer boundary, which allows the interdigitation of the terminal chains [57]. As a result, the rotation of the molecules about its short axis is hindered in HT cell, but imparts a significant influence in HG cell. Owing to the enhancement of the molecular size, the emergence of the P_2 mode has been observed in HG cell without bias field. By applying an external field, both of the compounds **1/9** and **1/10** clearly resolve the relaxation peak (P_2) in the planar anchoring Sm-$C_{(I)}$ phase as seen from Fig.

8.5(a) and Fig. 8.8(a). This mode is basically referred to a molecular mode arises due to rotation of molecules around their short axis. Additionally, this mode has an effect of the anti-ferroelectric organization of molecular dipoles. It has been observed that the mode P_2 is definitively absent in the compound **1/7**, while it appears in compound **1/9** after the application of external field and predominantly been found in the compound **1/10** without any bias field. This implies that by increasing the chain length, the molecular rotation is facilitating gradually about the short axis in case of HG cell. Therefore, it can be predicted that further increase of chain length should exhibit a noticeable appearance of this mode with a greater value of dielectric strength [56,58]. However, in case of HT cell, the direction of the effective dipole moment diverges from the field direction by increasing the chain length. In addition to this molecular rotation about the short axis is inhibiting by the enhancement of the chain length. As a result, prominently appearance of the mode H_1 in lower homologue turns out to an insignificant peak in the compound **1/10** which is clearly visible in the spectrum by the application of bias voltage (Fig. 8.8(b)). Therefore, the molecular motion becomes collective in the Sm-$C_{(I)}$ phase, *i.e.*, the relaxation process can be assumed due to the cooperative fluctuation of the dipoles. The associative arrangement of the molecules results an anti-ferroelectric ordering in adjacent layers which has also been found in other bent core-molecules [58,59]. However, the Sm-$C_{(II)}$ phase is like a glassy state or solid-like state which does not respond in external bias field. For deeper understanding of polar ordering for these smectic phases, the field induced switching behavior has also been studied which is described below.

8.4. Electro-optical investigation

The electro-optical investigation for the three investigated bent-core compounds has been carried out in combination with the field reversal polarization technique [60] by applying a triangular wave AC input voltage (amplified by 20 times) and simultaneous observation of the optical textures

(by using square wave) under a crossed polarizing optical microscope. An absolute voltage of 180 V_{pp}, 20 Hz has been applied with a proper resistive circuit to the sample filled ITO coated cells both in the planar and homeotropic orientations. Hence, an effective voltage of about ±20 V acts per μm on the cell which drives a current through the material. The output current spectrums have been acquired in Agilent DSOX2000A and the optical textures were observed by using a polarizing optical microscope (BANBROS) at a temperature interval of 1 K.

Out of the three investigated compounds, the lower homolog **1/7** has N_{CybC} and CybC phases where no prominent polarization peak has been detected throughout the mesomorphic range. On the other hand, the higher homologous compounds (**1/9** and **1/10**) exhibit two significant polarization peaks in the lower temperature smectic phases and a single polarization peak in the N_{CybC} phase, which exist also in the isotropic phase. The obtained current response spectrums along with the applied AC triangular wave voltage for the compounds **1/9** and **1/10** are depicted in Fig. 8.9(a-e) for both of the cell alignments. The corresponding temperature dependence values of the spontaneous polarization (P_s) are illustrated in Fig. 8.9(f,g). Simultaneous observations of optical textures in response to the applied square wave AC field are also represented in Fig. 8.10.

The output current spectrum for the planar-aligned compound **1/9** exhibits a broad asymmetrical current peak in the N_{CybC} phase even also in the isotropic phase as represented in Fig. 8.9(a) at different temperature above and below the I–N_{CybC} phase transition. However, an appearance of a sharp current peak has been observed in the HT configuration which is shown in the inset of Fig. 8.9(a). Similar observation has also been noticed in case of the compound **1/10** in the N_{CybC} phase for both the cell configurations. The area covered by the peak for both the compounds is sufficiently large near the isotropic phase

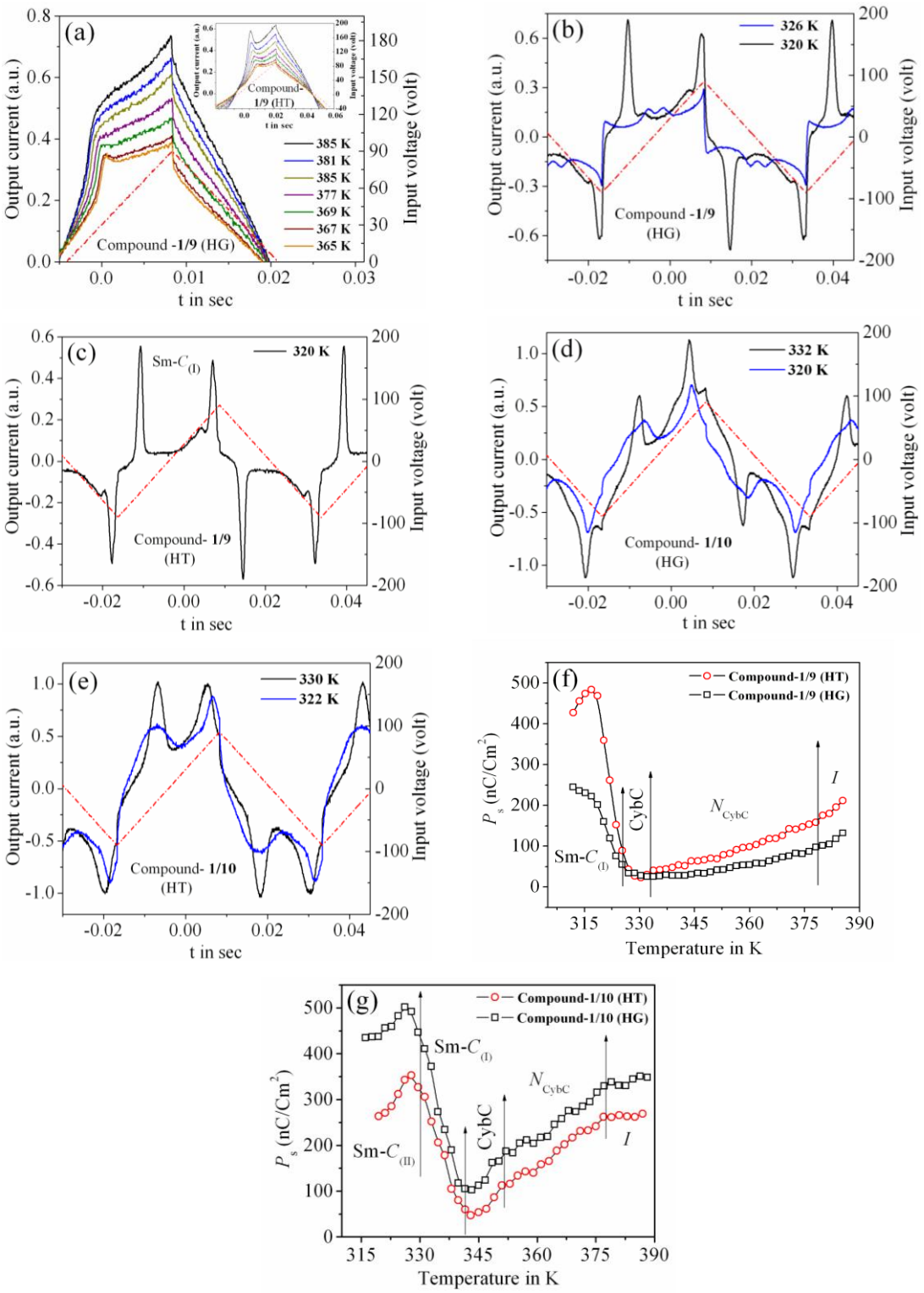

Figure 8.9. Switching current response curves of compound **1/9** and **1/10** for a triangular wave voltage (Red dashed line) at different temperatures; (a-c) Compound **1/9** in HG cell, (d) Compound **1/10** in HG cell, (e) Compound **1/10** in HT cell, (f-g) Temperature-dependent polarization value for the compound **1/9** and **1/10** respectively.

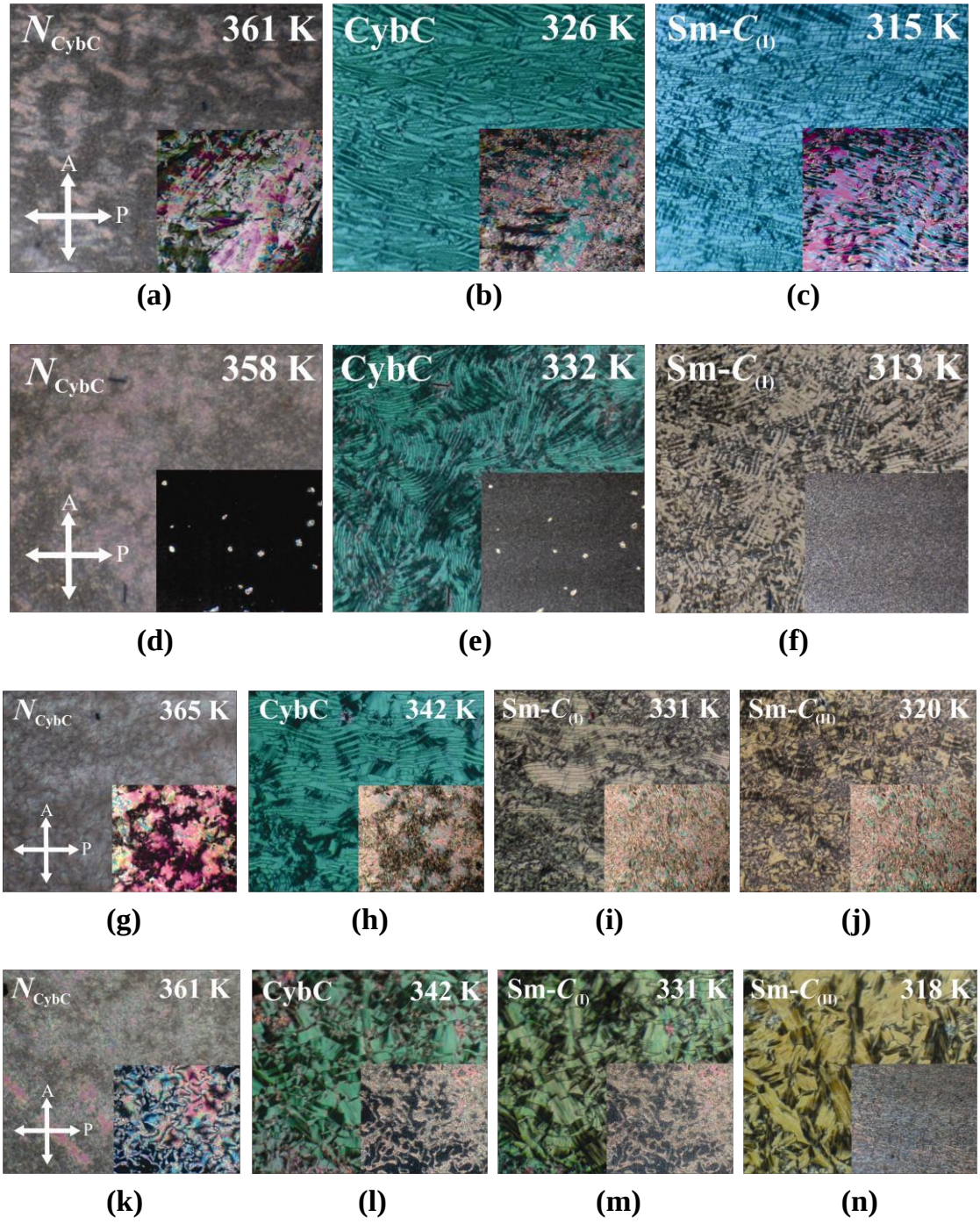

Figure 8.10. Optical textures of the compound **1/9** and **1/10** for an applied square wave AC voltage at different mesophases; (a-c): compound **1/9** in HG cell, (d-f): compound **1/9** in HT cell, (g-j): compound **1/10** in HG cell, (k-n): compound **1/10** in HT cell. Corresponding insets are the textures before the application of the field and arrows indicate the direction of the analyzer and polarizer.

and slowly diminishes in the N_{CybC} phase by lowering the temperature. Thus, the corresponding value of polarization (P_s) has been found to be about 210 nC/cm^2 in HT cell and about 140 nC/cm^2 in case of HG cell in the isotropic phase for the compound **1/9** (see Fig. 8.9(f)). On the other hand, the compound **1/10** reveals a quite higher value of about 320 nC/cm^2 in HG cell and about 260 nC/cm^2 in HT cell as represented in Fig. 8.9(g). Further lowering the temperature, the value of P_S gradually decreases throughout the entire N_{CybC} phase. Moreover, the application of a square wave input voltage (at different frequencies) also produces a hump in the output spectrum which eventually ruled out the emergence of this peak as ionic contribution. Rather it may be concluded that due to the existence of small clusters consisting of Sm-*C* type polar molecules in the N_{CybC} phase and even also in the isotropic phase induces such polarization peak. Quite similar type of observation has been reported in four-ring bent-core samples [61] and in the Sm-*A* phase of three-ring bent-core compound [62]. Therefore, the single peak observed in the switching current indicates that the fluctuation of the polarization vector of these polar cybotactic clusters is induced by the application of an external field, resulting in a ferroelectric-like polar switching [61,63,64] both in the isotropic and N_{CybC} phases. However, the average size of the polar clusters is very small near the isotropic phase which makes the reorientation of the dipolar axes quite easier and hence demonstrates a high value of polarization [30]. Moreover, as the temperature decreases the polar clusters grow up in size resulting in an effective increase of viscosity which also restricts the reorientation of the clusters within the N_{CybC} phase and hence the polarization value decreases by lowering the temperature. Subsequently, a sharp change of the planar-aligned schlieren nematic texture (inset of Fig. 8.10(a,g)) has been observed as shown in Fig. 8.10 (a,g) due to the application of an AC square wave field (180 V_{PP}, 5 Hz) in the N_{CybC} phase for both of the compounds. When the field is removed, the texture switches back into the initial state within a few milliseconds. Similar observation has also been found in HT cell as depicted in Fig.

8.10(d,k). Such ferroelectric nature in the nematic phase reveals a good consistency with several experimental reports [30,61,65] and often a quite higher value of polarization has also been reported in bent-core nematic phase [66]. As the polar clusters of the nematic phase are fused into elongated aggregates in the CybC phase, a ribbon-like optical texture arises in the CybC phase as a result of applied field which is depicted in Fig. 8.10(b,h) for HG cell and in Fig. 8.10(e,l) for the HT cell. Additionally, an appearance of two insignificant peaks in switching current has been found in this phase (blue curve in Fig. 8.9(b)). Further decreasing the temperature, two well distinct sharp peaks developed in the current response spectrum at the Sm-$C_{(I)}$ phase as shown in Fig. 8.9(b,c) for both the cell configurations. This is the signature of weak anti-ferroelectric ordering of the dipoles in adjacent layers. Nevertheless, the optical texture also shows a considerable change at the field-on state in the Sm-$C_{(I)}$ phase as represented in Fig. 8.10(c,i) for HG cell and Fig. 8.10(f,m) for the HT cell. Although the texture patterns are almost identical in the CybC and Sm-$C_{(I)}$ phases, a considerable change in the birefringence has been observed between these two phases. However, as the anti-parallel organization of the molecules in the neighboring layers is initiating from the CybC phase, the dual insignificant polarization peaks has found to appear from the CybC phase. On lowering the temperature, the obtained polarization value sharply increases to 250 nC/cm^2 for the HG configuration and 498 nC/cm^2 for the HT configuration in the Sm-$C_{(I)}$ phase as described in Fig. 8.9(f). Similar type of enhancement for the polarization value has also been reported in some bent-core anti-ferroelectric smectic phases [51,55,67-71]. Possibly, the steric interaction between the molecules reorients the terminal chains parallel to the layer boundary, which allows partial interlayer diffusion (interdigitation) of terminal chains [72]. Moreover, the strong dipole-dipole interaction also favors to align the molecular dipole moments in adjacent layers in an anti-parallel fashion. Combination of both the interaction stabilizes the anti-ferroelectric phase [72]. In addition, two well distinct sharp peaks of the compound **1/10** become

initially distorted in Sm-$C_{(II)}$ phase and finally disappears at a lower temperature as represented in Fig. 8.9(d,e) for the HG and HT cell configurations respectively. Moreover, the field-on optical texture in the Sm-$C_{(II)}$ phase eventually does not return to its initial state when the bias field is switched off as shown in Fig. 8.10(j,n) for the HG and HT cells respectively. This is essentially due to the effect of a more viscous medium with closely packed nature of the molecules in Sm-$C_{(II)}$ phase. Thus the Sm-$C_{(II)}$ phase corresponds to a more solid-like Sm-*C* phase or a glassy state. The value of the polarization increases with decrease in temperature having a maximum up to 520 nC/cm^2 for the HG configuration and 370 nC/cm^2 for the HT configuration in Sm-$C_{(I)}$ phase, while it decreases in the Sm-$C_{(II)}$ phase (see Fig. 8.9(g)). Surprisingly, the value of polarization for the compound **1/10** has found to be comparatively greater in case of HG cell than that of the HT cell in the lower temperature smectic phases, while the opposite nature has been observed in case of the second homologous compound **1/9**, *i.e.*, the value of polarization is greater for the HT cell than that of the HG cell. This unusual behavior can be explained by considering the deviation of resultant dipolar contribution with the variation of chain length in both the cell configurations. The magnitude of dipole moment for both the compounds are nearly equal, but owing to the elongation of chain length a strong component of the effective dipole moment is being oriented towards the direction of the field in the HG cell while it becomes weak in the HT cell. The obtained results in dielectric spectroscopy also support this behavior in which the first longitudinal peak (H_1) is absent in higher homologous compound (**1/10**), while a distinct appearance of second transverse mode (P_2) is observed in HG cell which is also observed in the planar-aligned compound **1/9**. Recently, a similar type of bent-core molecules (n = 6,8,12,14,16,18) has been synthesized from 4-cyanoresorcinol aromatic core [69,73-76] with the reversal of ester linking groups in which the higher homologous compounds (n = 16,18) possess a non-tilted and non-polar uniaxial Sm-*A* phase in addition to two uniform tilted Sm-*C* phases (Sm-C_SP_F and Sm-

C_SP_A) those are also exhibiting similar type of bulk polarization behavior. The field induced polarization study of present compounds (**1/9** and **1/10**) indicate that both lower temperature Sm-*C* phases are polar in nature with the anti-ferroelectric ordering of the dipoles and have a sufficiently high value of polarization (P_S). All these observations are found to be supportive with the conclusions made from the dielectric spectroscopy measurements. Finally, it appears that the Sm-$C_{(I)}$ phase should be designated as Sm-C_SP_A phase (C_S stands for synclinic-type of molecular organization and P_A corresponds to anti-ferroelectric ordering of polar orientation in neighboring layers) while Sm-$C_{(II)}$ phase is nothing but a quite solid-like state or close-packed Sm-*C* phase having another version of synclinic - anti-ferroelectric ordering (Sm-C'_SP_A phase).

8.5. Conclusion

Precise dielectric spectroscopy and electro-optical measurements have been performed to investigate the molecular dynamics for three homologous compounds (**1/7**, **1/9** and **1/10**) derived from 4-cyanoresorcinol bisbenzoates with terminally substituted varying alkyl chains (n = 7, 9, 10). All the compounds possess almost equal magnitude of dipole moment (~5.1 D). The lower homolog (**1/7**) comprises of a stable N_{CybC} phase in a broad temperature range, while the higher homologue (**1/9** and **1/10**) exhibit a N_{CybC} phase, in addition to tilted Sm-*C* phases- Sm-$C_{(I)}$ and Sm-$C_{(II)}$ followed by a CybC phase. The molecular conformations and their association impart a significant role in the mesomorphic behavior of the investigated compounds. Investigation on the dielectric spectroscopy for all of the compounds reveals that the compound **1/7** exhibits only one relaxation mode (P_1) in the planar-aligned N_{CybC} phase and ascribed as the molecular mode, arising due to the rotation of polar molecules around the long axis of the director within the Sm-*C* type tiny clusters. Besides, in HT cell, a couple of distinct relaxation modes has been found in which the low-frequency relaxation peak (H_1) appears due to the rotation of the molecules around their short axis and the higher frequency relaxation peak (H_2)

corresponds to the molecular mode associated with the local polar ordering of the molecules. However, the relaxation modes in N_{CybC} phase of the compound **1/9** have been found to be of similar nature as the relaxation modes (P_1, H_1 and H_2) of the lower homolog **1/7**. Interestingly, the dielectric strengths of these modes are too much sensitive to the externally applied bias field, indicating an influence of the effective dipole moment of the molecules on these modes. On the other hand, the higher homologous compound **1/10** exhibit only one longitudinal relaxation mode (H_2) throughout the mesmorphic region, which is also very sensitive to the applied bias field. Additionally, this compound exhibits two relaxation modes (P_1, P_2) in planar aligned Sm-$C_{(I)}$ phase. Due to the presence of a long terminal chain of the compound **1/10**, the steric interaction between the molecules reorients the terminal chains parallel to the layer boundary and forms an interdigitation of the terminal chains. This in effect restricts the rotational motion of the molecules around the short axis in HT cell and found to be gradually facilitating about the short axis in HG cell. More specifically it can be stated that due to the elongation of chain length a strong component of the effective dipole moment is being oriented towards the direction of the field in the HG cell while it becomes weaken in the HT cell. In order to investigate the polar contribution of these mesophases, the field reversal switching polarization has been measured in the investigated compounds over the whole mesomorphic range both in the HG and HT cell configurations. On the basis of all investigated results, it can be concluded that the N_{CybC} phase of these compounds mostly differ from the usual nematics, where a switchable macroscopic bulk polarization has been found in the direction of the applied electric field and defines a ferroelectric type of polar ordering. The molecules in the N_{CybC} phase are organized themselves in such a way that their individual dipoles suitably pile up to produce a large ferroelectric polarization within the medium. Moreover, the lower temperature Sm-*C* phases (Sm-$C_{(I)}$ and Sm-$C_{(II)}$) exhibit two well distinct peaks in current response curve, indicating an anti-ferroelectric type of ordering of the molecular dipoles in

adjacent layers. Due to this reason, the effective cancellation of the dipole moments reduces the dielectric strength ($\delta\varepsilon$) of the relaxation modes, but an application of an external bias voltage principally switches the dipoles along the field direction and hence significantly enhances the dielectric strength. The intermediate CybC phase endorsed the transition from the ferroelectric-type N_{CybC} phase to the anti-ferroelectric type of Sm-$C_{(I)}$ phase where the cybotactic clusters are being elongated. However, the Sm-$C_{(II)}$ phase is nothing but a Sm-*C* phase with enhanced packing density in comparison to Sm-$C_{(I)}$ phase, that seems like more solid-like state or glassy state. For this reason, even the field-on optical texture in the Sm-$C_{(II)}$ phase eventually does not return to its initial state as the field is completely switched off. Therefore, the development of polar order of the molecules in layers has been discussed in accordance with the variation of temperature and chain length. Considering all experimental findings it is concluded that the Sm-$C_{(I)}$ phase can be designated as Sm-C_SP_A (synclinic- anti-ferroelectric ordering) while the Sm-$C_{(II)}$ phase a quite solid-like state or close-packed Sm-*C* phase with similar type of synclinic - anti-ferroelectric ordering. This type of transition character from a rare ferroelectric N_{CybC} phase to anti-ferroelectric Sm-*C* phase is quite interesting among the bent-core molecules. All of the obtained outcomes emphasizes that these compounds may be used to formulate mixtures having improved material parameters like induced biaxialty, effective dipole moment, switching time etc. for practical applications.

References:

[1] F. Kremer, *J. Non-Cryst.* Solids, **305**, 1 (2002).

[2] O.E. Panarin, Y.P. Panarin, F. Antonelli, J.K. Vij, M. Reihmann, and G. Galli, *J. Matter. Chem.*, **16**, 842 (2006).

[3] U. Manna, J.-K. Song, Y.P. Panarin, A. Fukuda, and J.K. Vij, *Phys. Rev. E*, **77**, 041707 (2006).

[4] H. Xu, Y.P. Panarin, J.K. Vij, A.J. Seed, M. Hird, and J.W. Goodby, *J. Phys.: Condens. Mater*, **7**, 7443 (1995).

[5] Y.P. Panarin, H. Xu, S.T. MacLughadha, J.K. Vij, A.J. Seed, M. Hird, and J.W. Goodby, *J. Phys.: Condens. Matter*, **7**, L351 (1995).

[6] A. H. Price, and Á. Buka, in *Advances in Liquid Crystal Research and Applications*, edited by L. Bata, Pergamon Press, New York, Budapest (1980).

[7] H. Kresse, in *Physical Properties of Liquid Crystals: Nematics*, edited by D.A. Dunmur, A. Fukuda, and G. R. Luckhurst, Inspec, London (2001).

[8] L. Bata, and Á. Buka, *Acta Phys. Pol. A*, **54**, 635 (1978).

[9] Á. Buka, P.G. Owen, and A.H. Price, *Mol. Cryst. Liq. Cryst.*, **51**, 295 (1979).

[10] J. McConnell, in *Rotational Brownian motion and dielectric theory*, Academic Press, New York (1980).

[11] W.T. Coffey, and Y. P. Kalmykov, *Adv. Chem. Phys.*, **113**, 487 (2000).

[12] C. Krause, H. Yin, C. Cerclier, D. Morineau, A. Wurm, C. Schick, F. Emmerling, and A. Schonhals, *Soft Matter*, **8**, 11115 (2012).

[13] M. Marik, A. Mukherjee, D. Jana, A. Yoshizawa, and B.K. Chaudhuri, *Phys. Rev. E*, **88**, 012502 (2013).

[14] M.B. Pandey, R. Dhar, V.K. Agrawal, R.P. Khare, and R. Dabrowski, *Phase transit.*, **76**, 845 (2003).

[15] H. Takezoe, and Y. Takanishi, in *Smectic Liquid Crystals: antiferroelectric and ferrielectric phases*, H.S. Kitzerow, and C. Bahr (Eds.) in *Chirality in Liquid Crystals*, Springer-Verlag, Berlin (2001).

[16] R. Dabrowski, J.M. Oton, V. Urruchi, J.L. Gayo, K. Czuprynski, and S. Gauza, *Polish J. Chem.*, **76**, 331 (2002).

[17] M. Rajnak, P. Kopcansky, V. Gdovinova, V. Zavisova, I. Antal, J. Kurimsky, B. Dolnik, J. Jadzyn, N. Tomasovicova, M. Koneracka, and M. Timko, *Mol. Cryst. Liq. Cryst.*, **611**, 40 (2015).

[18] S. Kobayashi, T. Miyama, N. Nishida, Y. Sakai, H. Shiraki, Y. Shiraishi, and N. Toshima, *J. Disp. Technol.*, **2**, 121 (2006).

[19] G.P. Sinha, and F.M. Aliev, *Phys. Rev. E*, **58**, 2001 (1998).

[20] X.-L. Wu, W.I. Goldburg, M.X. Liu, and J.Z. Xue, *Phys. Rev. Lett.*, **69**, 470 (1992).

[21] Á. Buka, N. Éber , K. Fodor-Csorba , A. Jákli, and P. Salamon, *Phase Transit.*, **85**, 872 (2012).

[22] P. Salamon, N. Éber, Á. Buka, J.T. Gleeson, S. Sprunt, and A. Jákli, *Phys. Rev. E*, **81**, 031711 (2010).

[23] G. Pelzl, S. Diele, and W. Weissflog, *Adv. Mater.*, **11**, 707 (1999).

[24] S.K. Lee, S. Heo, J.G. Lee, K.-T. Kang, K. Kumazawa, K. Nishida, Y. Shimbo, Y. Takanishi, J. Watanabe, T. Doi, T. Takahashi, and H. Takezoe, *J. Am. Chem. Soc*., **127**, 11085 (2005).

[25] S. Kumar, and A.N. Gowda, *Liq. Cryst. Rev.*, **3**, 99 (2015).

[26] O. Francescangeli, V. Stanic, S.I. Torgova, A. Strigazzi, N. Scaramuzza, C. Ferrero, I.P. Dolbnya, T.M. Weiss, R. Berardi, L. Muccioli, S. Orlandi, and C. Zannoni, *Adv. Funct. Mater.*, **19**, 2592 (2009).

[27] E. Dorjgotov, K. Fodor-Csorba, J.T. Gleeson, S. Sprunt, and A. Jakli, *Liq. Cryst.*, **35**, 149 (2008).

[28] S. Stojadinovic, A. Adorjan, S. Sprunt, H. Sawade, and A. Jákli, *Phys. Rev. E*, **66**, 060701 (2002).

[29] D. Wiant, S. Stojadinovic, K. Neupane, S. Sharma, K. Fodor-Csorba, A. Jakli, J.T. Gleeson, and S. Sprunt, *Phys. Rev. E*, **73**, 030703 (2006).

[30] O. Francescangeli, V. Stanic, S. Torgova, A. Strigazzi, N. Scaramuzza, C. Ferrero, I.P. Dolbnya, T.M. Weiss, R. Berardi, L. Muccioli, S. Orlandi, and C. Zannoni, *Adv. Funct. Mater.*, **19**, 2592 (2009).

[31] O. Francescangeli, and E.T. Samulski, *Soft Matter*, **6**, 2413 (2010).

[32] O. Francescangeli, F. Vita, C. Ferrero, T. Dingemans, and E.T. Samulski, *Soft Matter*, **7**, 895 (2011).

[33] S. Chakraborty, J.T. Gleeson, A. Jákli, and S. Sprunt, *Soft Matter*, **9**, 1817 (2013).

[34] C. Zhang, M. Gao, N. Diorio, W. Weissflog, U. Baumeister, S. Sprunt, J.T. Gleeson, and A. Jákli, *Phys. Rev. Lett.*, **109**, 107802 (2012).

[35] S. Torgova, S.P. Sreenilayam, Y.P. Panarin, O. Francescangeli, F. Vita, J.K. Vij, E. Pozhidaev, M. Minchenko, C. Ferrero, and A. Strigazzi, *Phys. Chem. Chem. Phys.*, **19**, 22946 (2017).

[36] C. Keith, A. Lehmann, U. Baumeister, M. Prehm, and C. Tschierske, *Soft Matter*, **6**, 1704 (2010).

[37] D.R. Link, G. Natale, R. Shao, J.E. Maclennan, N.A. Clark, E. Körblova, and D.M. Walba, *Science*, **278**, 1924 (1997).

[38] G. Pelzl, S. Diele, and W. Weissflog, *Adv. Mater.*, **11**, 707 (1999).

[39] G. Shanker, M. Prehm, M. Nagaraj, J.K. Vij, M. Weyland, A. Eremin, and C. Tschierske, *Chem. Phys. Chem.*, **15**, 1323 (2014).

[40] G. Shanker, M. Nagaraj, A. Kocot, J.K. Vij, M. Prehm, and C. Tschierske, *Adv. Funct. Mater.*, **22**, 1671 (2012).

[41] A. Chakraborty, M.K. Das, B. Das, A. Lehmann, and C. Tschierske, *Soft Matter*, **9**, 4273 (2013).

[42] P. Perkowski, M. Mrukiewicz, K. Garbat, M. Laska, U. Chodorow, W. Piecek, R. Dabrowski, and J. Parka, *Liq. Cryst.*, **39**, 1237 (2012).

[43] M. Mrukiewicz, P. Perkowski, K. Garbat, R. Dabrowski, and J. Parka, *Acta Physica Polonica A*, **124**, 940 (2013).

[44] S. Havriliak, and S. Negami, *Polymer*, **8**, 161 (1967).

[45] S. Havriliak, and S. Negami, *J. Poly. Sci.*, **14**, 99 (1966).

[46] P. Nayek, S. Ghosh, S. Roy, T.P. Majumder, and R. Dabrowski, *J. Mol. Liq.*, **175**, 91 (2012).

[47] S. Ghosh, P. Nayek, S.K. Roy, T.P. Majumder, and R. Dabrowski, *Liq. Cryst.*, **37**, 369 (2010).

[48] Y. Jang, V.P. Panov, C. Keith, C. Tschierske, and J.K. Vij, *App. Phys. Lett.*, **97**, 152903 (2010).

[49] P. Tadapatri, U.M. Hiremath, C.V. Yelamaggad, and K.S. Krishnamurthy, *J. Phys. Chem. B*, **114**, 1745 (2010).

[50] P. Tadapatri, K.S. Krishnamurthy, and W. Weissflog, *Phys. Rev. E*, **82**, 031706 (2010).

[51] L. Kovalenko, M.W. Schröder, R.A. Reddy, S. Diele, G. Pelzl, and W. Weissflog, *Liq. Cryst.*, **32**, 857 (2005).

[52] P. Salamon, N. Eber, A. Buka, J.T. Gleeson, S. Sprunt, and A. Jákli, *Phys. Rev. E*, **81**, 031711 (2010).

[53] R. Balachandran, V.P. Panov, J.K. Vij, G. Shankar, C. Tschierske, K. Merkel, and A. Kocot, *Phys. Rev. E*, **90**, 032506 (2014).

[54] Y. Jang, V.P. Panov, A. Kocot, A. Lehmann, C. Tschierske, and J.K. Vij, *Phys. Rev. E*, **84**, 060701 (2011).

[55] A. Eremin, H. Nádasi, G. Pelzl, S. Diele, H. Kresse, W. Weissflog, and S. Grande, *Phys. Chem. Phys.*, **6**, 1290 (2004).

[56] L. Guo, K. Gomola, E. Grecka, D. Pociecha, S. Dhara, F. Araoka, K. Ishikawa, and H. Takezoe, *Soft Matter*, **7**, 2895 (2011).

[57] R.A. Reddy, and C. Tschierske, *J. Matter. Chem.*, **16**, 907 (2006).

[58] Y.P. Panarin, S.P. Sreenilayam, J.K. Vij, A. Lehmann, and C. Tschierske, *Beilstein J. Nanotechnol.*, **9**, 1288 (2018).

[59] H. Schlacken, P. Schiller, and H. Kresse, *Liq. Cryst.*, **28**, 1235 (2001).

[60] A. Pramanik, M.K. Das, B. Das, M. Żurowska, and R. Dabrowski, *Liq. Cryst.*, **42**, 412 (2015).

[61] S. Ghosh, N. Begum, S. Turlapati, S.K. Roy, A.K. Das, and N.V.S. Rao, *J. Mater. Chem. C*, **2**, 425 (2014).

[62] W. Weissflog, U. Baumeister, M.–G. Tamba, G. Pelzl, H. Kresse, R. Friedmann, G. Hempel, R. Kurz, M. Roos, K. Merzweiler, A. Jakli, C. Zhang, N. Diorio, R. Stannarius, A. Eremin, and U. Kornek, *Soft Matter*, **8**, 2671 (2012).

[63] G. Shanker, M. Prehm, M. Nagaraj, J.K. Vij, M. Weyland, A. Eremin, and C. Tschierske, *Chem. Phys. Chem.*, **15**, 1323 (2014).

[64] G. Shanker, M. Nagaraj, A. Kocot, J.K. Vij, M. Prehm, and C. Tschierske, *Adv. Funct. Mater.*, **22**, 1671 (2012).

[65] S. Turlapati, R.K. Khan, S. Ghosh, P. Tadapatri, R. Pratibha, and N.V.S. Rao, *Journal of Applied Physics*, **120**, 174101 (2016).

[66] O. Francescangeli, F. Vita, and E.T. Samulski, *Soft Matter*, **10**, 7685 (2014).

[67] N. Sebastian, S. Belau, A. Eremin, M. Alasar, M. Prehm, and C. Tschierske, *Phys. Chem. Chem. Phys.*, **19**, 5895 (2017).

[68] S. Sreenilayam, M. Nagaraj, Y.P. Panarin, J.K. Vij, A. Lehmann, and C. Tschierske, *Mol. Cryst. Liq. Cryst.*, **553**, 140 (2012).

[69] C. Keith, M. Prehm, Y.P. Panarin, J.K. Vij, and C. Tschierske, *Chem. Commun*., **46**, 3702 (2010).

[70] M. Alaasar, M. Prehm, S. Poppe, and C. Tschierske, *Chem. Eur. J*, **23**, 5541 (2017).

[71] S.P. Sreenilayam, Y.P. Panarin, J.K. Vij, A. Lehmann, M. Poppe, and C. Tschierske, *Phys. Rev. Materials*, **1**, 035604 (2017).

[72] K. Nishida, M. Čepič, W.J. Kim, S.K. Lee, S. Heo, J.G. Lee, Y. Takanishi, K. Ishikawa, K.-T. Kang, J. Watanabe, and H. Takezoe, *Phys. Rev. E*, **74**, 021704 (2006).

[73] M. Nagaraj, Y.P. Panarin, J.K. Vij, C. Keith, and C. Tschierske, *App. Phys. Lett.*, **97**, 213505 (2010).

[74] S. Sreenilayam, Y.P. Panarin, J.K. Vij, M. Osipov, A. Lehmann, and C. Tschierske, *Phys. Rev. E*, **88**, 012504 (2013).

[75] Y.P. Panarin, M. Nagaraj, J.K. Vij, C. Keith, and C. Tschierske, *Europhys. Lett.*, **92**, 26002 (2010).

[76] S.P. Sreenilayam, Y.P. Panarin, J.K. Vij, P. Panov, A. Lehmann, M. Poppe, M. Prehm, and C. Tschierske, *Nature Comm.*, **7**, 11369 (2016).